Morphological Characterization of Self-Assembled Peptide Nucleic Acid Amphiphiles

Cheryl Lau,[†] **Ronit Bitton,**[‡] **Havazelet Bianco-Peled,**[§] **David G. Schultz,**[∥] **David J. Cookson,**[⊥] **Shane T. Grosser,**[†] **and James W. Schneider*,**[†]

Department of Chemical Engineering, Carnegie Mellon University, Pittsburgh, Pennsylvania 15213-3890, Inter-Departmental Program for Biotechnology and Department of Chemical Engineering, Technion—Israel Institute of Technology, Haifa 32000, Israel, Department of Physics, University of Illinois at Chicago, Chicago, Illinois 60607, and Australian Synchrotron Research Program, Building 434, Argonne, Illinois 60439

Peptide nucleic acid amphiphiles (PNAA) are a promising set of materials for sequence-specific separation of nucleic acids from complex mixtures. To implement PNAA in micellar separations, the morphology and size of PNAA micelles in the presence and absence of a sodium dodecyl sulfate (SDS) cosurfactant have been studied by small-angle X-ray scattering and dynamic light scattering. We find that a 6-mer PNAA with a 12-carbon *n*-alkane tail forms ellipsoidal micelles ($a = 5.15$ nm; $b = 3.20$ nm) above its critical micelle concentration (CMC) of 110.9 μM. On addition of a stoichiometric amount of complementary DNA, PNAA hybridizes to DNA, suppressing the formation of PNAA micelles. At a ratio of 19:1 SDS/PNAA (total concentration = 20 mM), spherical micelles are formed with outer radius $R_s = 2.67$ nm, slightly larger than spherical micelles of pure SDS. Capillary electrophoresis studies show that PNAA/DNA duplexes do not comicellize with SDS micelles. No such effects are observed using noncomplementary DNA. The shape and size of the PNAA micelles is also verified by dynamic light scattering (DLS) studies. These results provide an interesting case study with competing electrostatic, hydrophobic, and hydrogen-bonding interactions in micellar systems and make possible the use of PNAA in micellar separations of DNA oligomers.

Introduction

Self-assembly is an attractive route for the synthesis of functional nanomaterials, requiring minimal intervention and providing a wide range of useful morphologies depending on solution conditions. Self-assembling systems with useful bioactivity can be created by linking lipophilic moieties to bioactive peptides to form peptide amphiphiles. In addition to forming monolayers at various interfaces, appropriately designed peptide amphiphiles will micellize above their critical aggregation concentration. Peptide amphiphiles have been shown to assemble into micellar spheres,[1] disks,[1] rods,[2] or helical ribbons,[3] depending on the building blocks of the micelle and solution conditions. Scattering methods such as dynamic light scattering (DLS),[4,5] small-angle neutron scattering (SANS),[1] and small-angle X-ray scattering (SAXS)[6–10] have been employed widely for determining the size, shape, and structure of micelles.

We have been investigating the use of peptide amphiphiles for bioseparations and biosensing applications, particularly electrokinetic separations amenable to microchip analysis. The electrophoretic mobility of micelles is a function of their charge and hydrodynamic radius (r_H). Since rodlike or ellipsoidal micelles will have a larger r_H than spherical micelles for the same aggregation number, knowledge of the micelle morphology is critical to the design of electrokinetic separation systems using micelles. One such format, micellar electrokinetic chromatography (MEKC), uses a large excess of micelles in the capillary running buffer as a pseudostationary phase. For these systems, morphological characterization of mixed micelles is essential.

We have developed a class of peptide amphiphiles that hybridize to particular DNA sequences, tagging them for removal from complex mixtures.[11–13] Hybridization is achieved through the use of a peptide nucleic acid (PNA) group. PNAs are synthetic DNA mimics that bind DNA and RNA complements with high stability and sequence selectivity.[14] The self-assembly of PNA amphiphiles (PNAA) is facilitated by the lack of charge on the backbone of the PNA peptide, limiting electrostatic repulsion between headgroups in assembled structures.

Like PNA peptides, PNAA bind DNA in a sequence-specific way, with binding thermodynamics and binding specificity unaffected by the presence of the aliphatic tail.[11] Moreover, the presence of the aliphatic tail greatly improves the separation resolution of PNAA/DNA complexes from unbound DNA in liquid chromatography.[12] The development of PNAA micelles would also enable the application of micellar electrokinetic chromatography (MEKC) separation,[15,16] a mode of capillary electrophoresis (CE). Furthermore, a mixed micelle of PNAA and a cosurfactant would allow for the fine-tuning of electrophoretic mobility, while spacing apart the PNAA peptides and the bound duplex for improved resolution.

Here, we use small-angle X-ray scattering (SAXS) to determine the morphology of PNAA on their own, in the presence of cosurfactants suitable for MEKC, and in the presence of DNA oligomers complementary to the PNAA. Substantial differences in the critical micelle concentration and

* To whom correspondence should be addressed. E-mail: schneider@cmu.edu.
† Carnegie Mellon University.
‡ Inter-Departmental Program for Biotechnology, Technion—Israel Institute of Technology.
§ Department of Chemical Engineering, Technion—Israel Institute of Technology.
∥ University of Illinois at Chicago.
⊥ Australian Synchrotron Research Program.

9028 *J. Phys. Chem. B, Vol. 110, No. 18, 2006*

Lau et al.
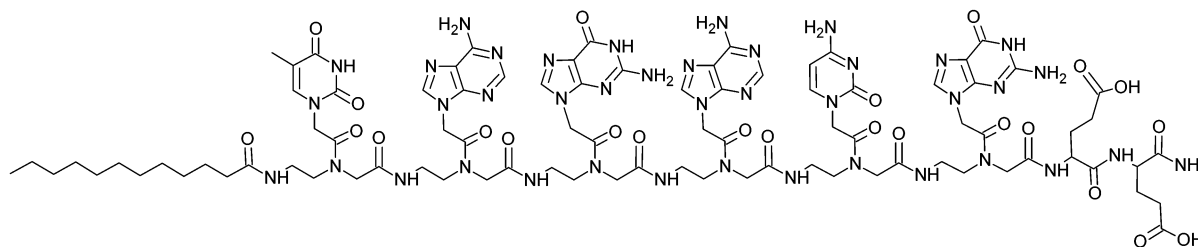
Figure 1. Chemical structure of the PNA amphiphile "C_{12}-tagacg-$(E)_2$". The structure is listed from N to C terminus (left to right) or from the 5′ to 3′ end of a corresponding oligomer of DNA.

micelle morphology result as the balance of hydrophobic, electrostatic, and hydrogen-bonding forces is shifted under these conditions.

Materials and Methods

Sodium dodecyl sulfate (SDS, MW = 288.38) and all solvents (sequencing grade) used in this study were purchased from Fisher Scientific (Pittsburgh, PA). All PNA monomers and reagents were acquired from Applied Biosystems (Foster City, CA). Fmoc-protected PAL-PEG-PS resin from Peptides International (Louisville, KY) with a 0.21 mmol/g loading capacity was used. Synthetic DNA oligonucleotides (1 μmol scale) were obtained from Integrated DNA Technologies, Inc. (Coralville, IA) as lyophilized solids and were used without further purification.

Synthesis of PNA Amphiphiles (PNAA). PNAA (C_{12}-tagacg-$(E)_2$, Figure 1) was synthesized on a Fmoc-protected PAL-PEG-PS resin with standard solid-phase protocols.[17] For a 6-base-pair PNA with a single, 12-carbon alkyl tail, it was found that the addition of two glutamic groups showed good solubility in different solution conditions. Glutamic acid was added to the C-terminus of PNA as the first coupling reaction. Finally, lauric acid was added to the N-terminus of PNA as the last step in the synthesis to provide the hydrophobicity. The crude product was then purified by reversed-phase high-performance liquid chromatography (HPLC) on a Delta 600 HPLC (Waters) using a reverse-phase Symmetry300 C_4 column with a particle size of 5 μm. The product was verified by MALDI-TOF mass spectrometry (MS) using a Voyager STR spectrometer (PerSeptive) with an α-cyano-4-hydroxycinnamic acid matrix (theoretical MW = 2108.12; experimental [M + H]$^+$ = 2109.6, [M + Na]$^+$ = 2131.6).

Critical Micelle Concentration (CMC) Determination. The concentration of PNAA micelles [M] as a function of total PNAA [S_T] was determined by a dye solubilization method using the fluorescent dye nile red (Sigma Aldrich, MW = 318.39). Fluorescence measurements were made on small samples of PNAA solutions (25 μL total volume) using a SpectraMax M3 microplate reader with a xenon flash lamp source (Molecular Devices). The dye was dissolved in methanol (2.5 mg/mL) and then diluted to 200 μM using 50 mM Tris-HCl buffer (pH 8.0) to serve as a stock solution. A 12.5 μL portion of 200 μM nile red dye and a 12.5 μL portion of a PNAA sample (varying concentration) were placed in each well of a 96-well plate. The total concentration of PNAA in each well was varied from 0 to 1 mM in 2.5−50 μM increments. After 24 h (to ensure complete solubilization of nile red), the fluorescence intensity at 636 nm was measured for each well using an excitation wavelength of 550 nm. The resulting intensity versus [PNAA] plots were analyzed to obtain the total CMC. Since the monomer-to-micelle transition was broad, the closed-association model was used to fit the data. For a system with only monomers at a concentration [S] and micelles [M],

an equilibrium constant for micellization is defined as[18]

$$K_M = \frac{[M]}{[S]^N} \tag{1}$$

The critical micelle concentration (CMC) is given by

$$CMC = \left(\frac{N^2[M]}{([S_T] - N[M])^N} \right)^{1/(1-N)} \left(1 + \frac{1}{N} \right) \tag{2}$$

The partitioning of dye to the micellar pseudophase is described by a partition coefficient K:

$$K = \frac{[D_M]}{[D_{aq}][M]} \tag{3}$$

Here, [S_T] is the surfactant concentration, and [D_{aq}] and [D_M] are the concentrations of dye in the aqueous phase and micellar pseudophase, respectively. Since the total amount of dye is specified ([D_T] = [D_{aq}] + [D_M]), we have

$$\frac{[D_M]}{[D_T]} = \frac{K[M]}{1 + K[M]} = \frac{I - I_o}{I_\infty - I_o} \tag{4}$$

where I is the measured fluorescence intensity, I_∞ is the intensity corresponding to complete dye solubilization, and I_o is the background intensity from the dye in the absence of surfactant. With the experimental data I, I_o, and [S_T], eqs 2 and 4 were solved implicitly by an optimization algorithm (IPOPT)[19] to obtain the unknown parameters: CMC, N, K, and I_∞.

Capillary Electrophoresis (CE). DNA oligomers were obtained from Integrated DNA Technologies (Coralville, IA) and used as received. Stock solutions of DNA (approximately 1 mM, this concentration was quantified precisely by UV absorbance) in 50 mM Tris-HCl buffer (pH 8.0) were prepared. CE was carried out in a Beckman P/ACE MDQ CE system equipped with a UV detector and a liquid-cooled capillary cartridge. Experiments were performed in a fused silica capillary (50 μm i.d., 21.0 cm in length to a detector, l, 31.2 cm total length) at 22 °C. Sample solutions of ~1 mM of DNA and 1 mM of PNAA in 50 mM Tris-HCl buffer (pH 8.0) were prepared from the stock solution. Samples were introduced into the capillary by hydrodynamic injection (0.5 psi for 5 s) and eluted under normal polarity with an electric field of 240 V/cm using a running buffer of pH 8.0 Tris-HCl. Samples were detected at 254 nm, and a neutral marker (50 μM benzyl alcohol) was used in each run to determine the magnitude of electro-osmotic flow (EOF) in the uncoated capillary. The electrophoretic mobility (μ) of the sample was calculated from retention time (t) data by the following:

$$\mu = \frac{l(t_o - t_s)}{Et_o t_s} \tag{5}$$

where l is the effective length of the capillary, E is the electric field, and t_s and t_o are the retention times of the sample and a neutral marker, respectively.

Small-Angle X-ray Scattering (SAXS) Experiments. SAXS measurements were performed using a slit-collimated compact Kratky camera (A. Paar Co.) at the Technion–Israel Institute of Technology. The entrance slit to the collimating block was 40 μm, and the slit length delimiters were set at 15 mm. Ni filtered CuKα ($\lambda = 1.542$ Å) radiation was generated by a sealed-tube source (Philips). Samples were placed in cylindrical quartz cells (A. Paar Co., 1 mm path length), and their temperature was kept constant ($T = 25$ °C) by means of a temperature controller (A. Paar Co.). The flight path was kept under vacuum, with a sample-to-detector distance of 26.4 cm. Scattering was measured with a linear position sensitive detector system (Raytech, gold-coated tungsten wire in a stream of 90% Ar + 10% CH$_4$ gas at 3 bar), with pulse-height discrimination and a multichannel analyzer (Nucleus). A total of 3000 or more counts for each channel were collected in order to obtain a low signal-to-noise ratio. Primary beam intensities were determined using the moving slit method of Stabinger and Kratky[20] and subsequently using a thin quartz monitor as a secondary standard. The scattering curves, as a function of the scattering vector $q = 4\pi \sin \theta / \lambda$ (where 2θ and λ are the scattering angle and the wavelength, respectively), were corrected for counting time and for sample absorption. The background scattering was determined separately using a buffer-filled capillary and subtracted from the experimental curve. To rectify the effects of the beam dimensions, a desmearing procedure was performed according to the indirect transformation method.[21] Data analysis was based on fitting the desmeared curve to an appropriate model using a least-squares procedure.

Synchrotron SAXS measurements were carried out at the ChemMatCARS sector of the Advanced Photon Source. A photon energy of 8.27 keV ($\Delta E/E = 10^{-4}$) was obtained by use of a double-crystal diamond monochromator. Vertical (1:1) focusing was achieved with a set of mirrors upstream of the sample. The beam size at the sample was 500×300 μm^2 (horizontal $\times$ vertical), with a corresponding flux of 3×10^{12} photons/s. Three sets of slits before the sample were carefully aligned to define the beam size and reduce parasitic scattering. The SAXS camera consisted of a variable length vacuum tube equipped with a Bruker 6000 CCD detector (92 μm pixel size, 94×94 mm^2 area). This setup enabled measurements of length scales ranging from a few angstroms to a few hundred nanometers. Samples were held in thin-walled quartz capillaries (i.d. = 1.5 mm). All data was corrected by background subtraction of the appropriate buffer solution. Care was taken to collect pure water, buffer, and sample signals in the same capillary. In this way, the water signal was used to scale the background-corrected sample data to absolute intensity units.

SAXS Modeling. The scattering intensity from a dilute particulate system can be regarded as the sum of the intensities scattered by the individual particles. For a monodisperse system of particles of identical shape, the total scattering intensity per unit volume of sample $i(q)$, normalized to the scattering intensity of a single electron is given by[21]

$$I(q) = N_p P(q) \tag{6}$$

where q is the scattering vector, N_p is the number of particles

per unit volume, and $P(q)$ is the form factor of a single particle. The total intensity scattered from a polydisperse system with particles having an identical shape can be described by

$$I(q) = \int_0^\infty D_n(R) \, P(q,R) \, dR \tag{7}$$

where $D_n(R) \, dR$ is the number of particles whose size is between R and $R + dR$ per unit volume of sample. A core–shell model was used in which the micelle is divided into two parts: a core consisting of hydrophobic tails with constant electron density ρ_c and a shell consisting of headgroups with constant electron density ρ_s. Substitution of the form factor for a core–shell sphere into eq 7 yields[22]

$$I(q) = N_p[V_c(\rho_c - \rho_s)\Phi(qR_c) + V_s(\rho_s - \rho_{solv})\Phi(qR_s)]^2 \tag{8}$$

where R_c is the radius of the core, R_s is the radius of the shell, and

$$\Phi(qR) = 3\frac{\sin(qR) - qR \cos(qR)}{(qR)^3} \tag{9}$$

Polydispersity is accounted for by averaging $P(q)$ over a Schulz distribution of radii, holding the ratio R_c/R_s constant. Substitution of the form factor for a core–shell prolate ellipsoid into eq 7 yields

$$I(q) = N_p\int_0^1 |V_{core}(\rho_{shell} - \rho_{core})\frac{3j_1(u_{core})}{u_{core}} +$$
$$V_{shell}(\rho_{solv} - \rho_{shell})\frac{3j_1(u_{shell})}{u_{shell}}|^2 \, d\alpha + bkg \tag{10}$$

$$u_x = q[r_{x,maj}^2\alpha^2 + r_{x,min}^2(1 - \alpha^2)]^{1/2} \tag{11}$$

$$V_x = \frac{4\pi}{3}r_{x,maj}r_{x,min}^2 \tag{12}$$

$$j_1(x) = \frac{(\sin x - x \cos x)}{x^2} \tag{13}$$

Here, V is the volume, ρ is the electron density, $r_{x,maj}$ is the ellipsoid major axis, $r_{x,min}$ is the ellipsoid minor axis, and bkg is the instrumental background (α is an integration variable).

Dynamic Light Scattering (DLS) Experiments. A Zetasizer 3000HS (Malvern Instruments) with a 10 mW helium–neon laser source (632.8 nm) was used for the experiments. The intensity of light scattered at 90° from incidence is measured by a photomultiplier tube and directed to a correlator. The instrument software derives particle size from the time correlation function and calculates the diffusion coefficient from the slope of decay rate (r) versus q^2 plot. All sample solutions were passed through a 0.1 μm filter (Whatman) to exclude dust particles. Measurements were performed in triplicate, and the accuracy of the instrument was verified using suspensions of latex beads of a known diameter (60 and 200 nm, Duke Scientific).

DLS measures the normalized intensity–intensity time autocorrelation function $g_2(r)$ through a correlator:

$$g_2(r) = A(1 + B|g_1(\tau)|^2) \tag{14}$$

where A, B, and $|g_1(\tau)|$ are the background, coherent factor, and normalized electric field autocorrelation function. The
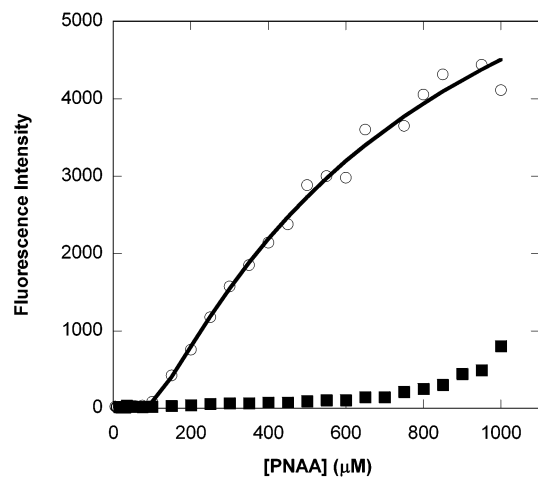
Figure 2. Fluoresence intensity ($\lambda_{\text{excitation}} = 550$ nm, $\lambda_{\text{emission}} = 636$ nm) for PNAA (open circles) in the presence of 100 μM nile red dye (50 mM Tris-HCl, pH 8.0). A simultaneous fit to a dye-partitioning model and the closed-association model for micellization (solid line) yields the following: CMC = 110.9 μM, N = 10, K = 0.01, I_∞ = 8657. The closed squares represent data under the same conditions but in the presence of 1 mM complementary DNA (5'-CGTCTA-3').

function $|g_1(\tau)|$ can be analyzed through various fitting methods, e.g., CONTIN, NNLS, etc., to yield the decay rate r. Assuming that there is no internal motion, the apparent diffusion coefficient D_{app} can be obtained by the following relation:

$$D_{\text{app}} = r/q^2 \tag{15}$$

In general, D_{app} is concentration dependent. The diffusion coefficient at infinite dilution is given by the Stokes−Einstein equation:

$$D_{\text{o}} = \frac{kT}{6\pi\eta R_{\text{H}}} \tag{16}$$

where k is Boltzmann's constant, η is the solvent viscosity (water, 0.0089 P at T = 25 °C), and R_{H} is the hydrodynamic radius of an equivalent sphere. For a prolate ellipsoid, the hydrodynamic radius is given by[24]

$$R_{\text{H}} = \frac{b\sqrt{(1 - x^2)}}{\ln\left(\dfrac{1 + \sqrt{(1 - x^2)}}{x}\right)} \tag{17}$$

where a is the semiminor axis, b is the semimajor axis, and x = a/b.

Results and Discussion

PNAA of different structures can be synthesized with full control over the sequence and length of the peptide headgroup. In this paper, we mainly focus on a short PNAA molecule, C_{12}-tagacg-$(E)_2$ (Figure 1). The short sequence made producing larger quantities of PNAA possible while preserving the ability to hybridize DNA. A van't Hoff analysis of UV thermal scans gave a T_m of 25.3 °C for an equimolar solution of C_{12}-tagacg-$(E)_2$ and its 6-mer DNA complement. Self-assembly of the PNAA was monitored using a nile-red dye solubilization method (Figure 2) under the assumption that fluorescence intensity linearly increases with the concentration of micelles. Fits of the intensity vs concentration plots to the closed-association model of micellization (eq 4) yield a value of 110.9 μM for the CMC
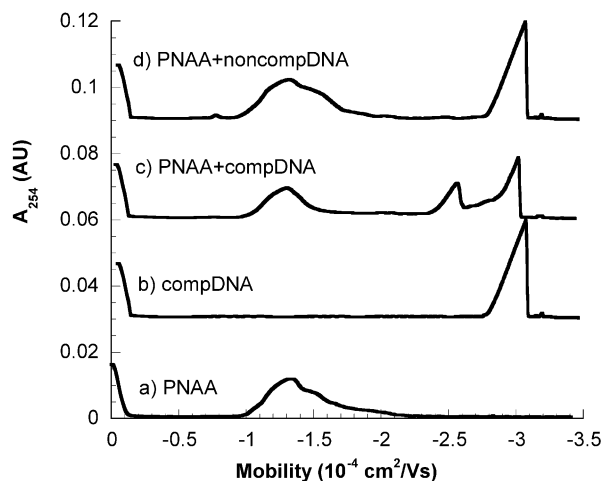
Figure 3. Capillary electropherogram for (a) 1 mM PNAA, (b) 1 mM complementary DNA (5'-CGTCTA-3'), (c) 1 mM PNAA and 1 mM complementary DNA, and (d) 1 mM PNAA and 1 mM noncomplementary DNA (5'-GCAGAT-3'). All samples are in 50 mM Tris-HCl buffer (pH 8.0). The shoulder at mobility = 0 represents half the neutral marker peak (see text).

and an aggregation number (N) of 10. The broadness of the transition indicates the presence of aggregates well below the nominal CMC value. On addition of 1000 μM of complementary DNA, formation of PNAA micelles (as judged by an increase in the fluorescence intensity) is not observed until a concentration of about 700 μM of PNAA is achieved. This corresponds to a shift of about 590 μM, about the amount of PNAA expected to hybridize with DNA at this temperature. Additionally, data obtained using 1000 μM of a noncomplementary DNA 6-mer showed no such shift in the intensity vs concentration plot.

These results indicate that the PNAA/DNA duplexes do not micellize, while the unbound PNAA do. Since the PNAA and DNA were mixed together from stock solutions of the pure compounds, the PNAA must first have been present as a mixture of PNAA monomers and micelles. It is not clear whether DNA hybridization to PNAA monomer is favored over PNAA in micelles, but one could expect that equilibrium between all components would be established fairly quickly since the kinetics for most micellization and hybridization processes are much faster than the time scale of the experiment (hours). While not extensively tested, we did not observe any effect of solution mixing or incubation history on the dye solubilization results, supporting this assertion. For discussion purposes, we will refer to the hybridization-induced shifting of equilibrium away from the micelle pseudophase as "transfer" of the PNAA to solution.

The extent of PNAA/DNA binding as well as micellization can be tracked using capillary electrophoresis. Figure 3 shows electropherograms for PNAA (1 mM) with an equimolar amount of complementary and noncomplementary DNA. To account for small changes in electro-osmotic flow from run to run, absorbance is plotted against electrophoretic mobility (μ) rather than migration time (eq 5). Since electrophoresis is directed against electro-osmosis for the negatively charged PNAA, DNA, and SDS, longer migration times indicate higher electrophoretic mobility.

The PNAA on its own (Figure 3a) shows a broad peak at about -1 to -2×10^{-4} cm²/(V s), while the complementary DNA (Figure 3b) has a single, well-defined peak at about -3×10^{-4} cm²/(V s). Some of the skew in the peaks, particularly for the DNA, can be attributed to electrodispersion effects, as the chloride ion of the Tris-HCl buffer has a much higher mobility than either analyte, leading to inhomogeneous electric

TABLE 1: Thermodynamic Data for Hybridization of PNAA C_{12}-tagacg-$(E)_2$ with Complementary DNA Oligomer 5′-CGTCTA-3′ [a]

T_m (°C)	ΔH (kcal/mol)	ΔS (cal/(mol K))
25.2	−51.5	−147

[a] Values are averaged over heating and cooling cycles with [PNAA] = [DNA] = 5 μM (10 mM phosphate buffer, pH 7.0).
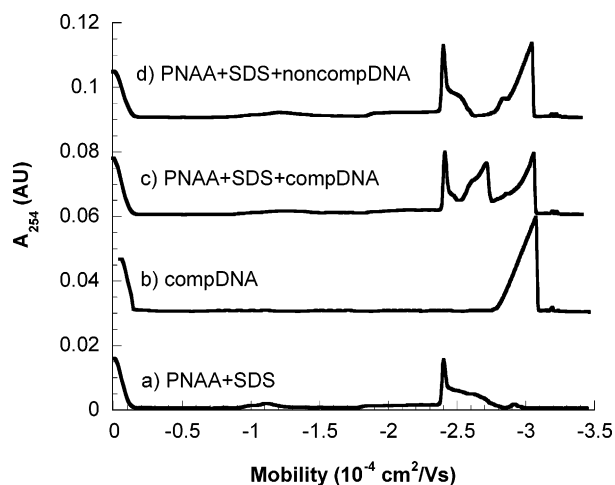

Figure 4. Capillary electropherogram for (a) 1 mM PNAA and 19 mM SDS; (b) 1 mM complementary DNA (5′-CGTCTA-3′); (c) 1 mM PNAA, 1 mM complementary DNA, and 19 mM SDS; (d) 1 mM PNAA, 1 mM noncomplementary DNA (5′-GCAGAT-3′), and 19 mM SDS. All samples are in 50 mM Tris-HCl buffer (pH 8.0). The shoulder at mobility = 0 represents half the neutral marker peak (see text).

fields in the capillary.[25] On addition of complementary DNA to PNAA (Figure 3c), a third peak emerges at -2.5×10^{-4} cm²/(V s), corresponding to the PNAA/DNA duplex. The mobility is lower than that of unbound DNA, as expected for the addition of PNAA with a much lower charged density than DNA. The shape of the PNAA/DNA peak is much more similar to the unbound DNA peak than the peak corresponding to PNAA micelles, supporting the idea that PNAA micelle formation is suppressed on DNA hybridization to PNAA. On addition of noncomplementary DNA (Figure 3d), a superposition of Figure 3a and b is observed, indicating no interaction between the PNAA and DNA. The transfer of PNAA from the micelle phase on DNA hybridization appears to be a specific process. Note that only about half the PNAA hybridizes to complementary DNA as expected (T_m = 25.2 °C, Table 1).

Comicellization of PNAA with SDS. Sodium dodecyl sulfate (SDS) is a typical surfactant used as a pseudostationary phase in MEKC. To study its micellization properties with PNAA, we conducted CE measurements on the PNAA ([PNAA] = 1 mM) in the presence of SDS at concentrations well above its CMC ([SDS] = 19 mM). Figure 4a is an electropherogram for PNAA with SDS, showing a shift in mobility to about -2.4×10^{-4} cm²/(V s), indicating the formation of a mixed micelle with a higher mobility than PNAA micelles. On addition of complementary DNA (Figure 4c), a third peak again emerges as the PNAA/DNA duplexes are formed, indicating that the duplexes do not adsorb or comicellize with SDS micelles. Again, addition of noncomplementary DNA yields a superposition of Figure 4a and b, highlighting the specificity of the process.

SAXS Characterization for Pure and Mixed Micelles of PNAA. With an eye toward predicting the electrophoretic mobility of PNAA micelles, small-angle X-ray scattering studies were undertaken. Our first studies were conducted using a CuKα source. Figures 5 and 6 show the desmeared scattering curves,
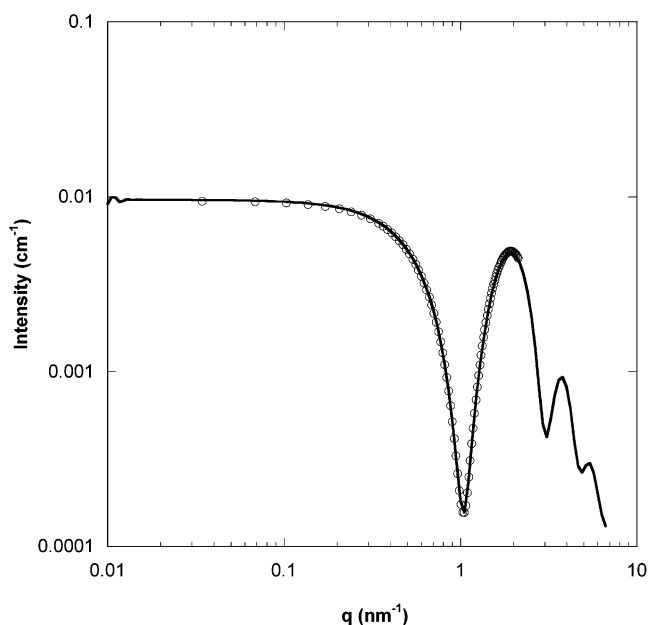

Figure 5. Desmeared CuKα SAXS intensities for 19 mM SDS in 50 mM Tris-HCl buffer (pH 8.0). The solid line is a fit using the polydisperse core−shell spherical model (eq 8) with the parameters in Table 2. Intensity is plotted in units of inverse centimeters for comparison to Figure 7.
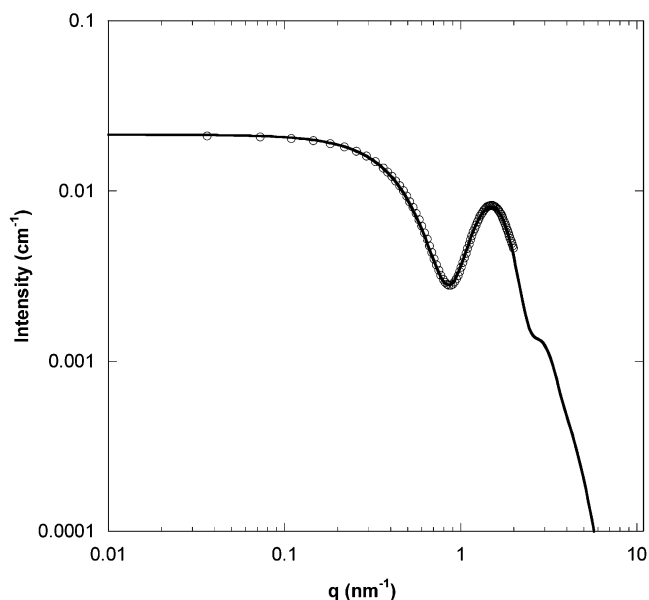
Figure 6. Desmeared CuKα SAXS intensities for a mixture of 1 mM PNAA (Figure 1) and 19 mM SDS in 50 mM Tris-HCl buffer (pH 8.0). The solid line is a fit using the polydisperse core−shell spherical model (eq 8) with the parameters in Table 2. Intensity is plotted in units of inverse centimeters for comparison to Figure 7.

plotted as the scattering cross section versus the scattering vector (q) in nanometers. We note that the Kratky camera employed signal averages over a substantial volume; it cannot give a true scattering cross section, and absolute intensity (I) in electrons squared per cubic centimeter is typically plotted to reflect this. In our case, we used units of inverse centimeters simply for comparison to synchrotron X-ray data (Figure 7).
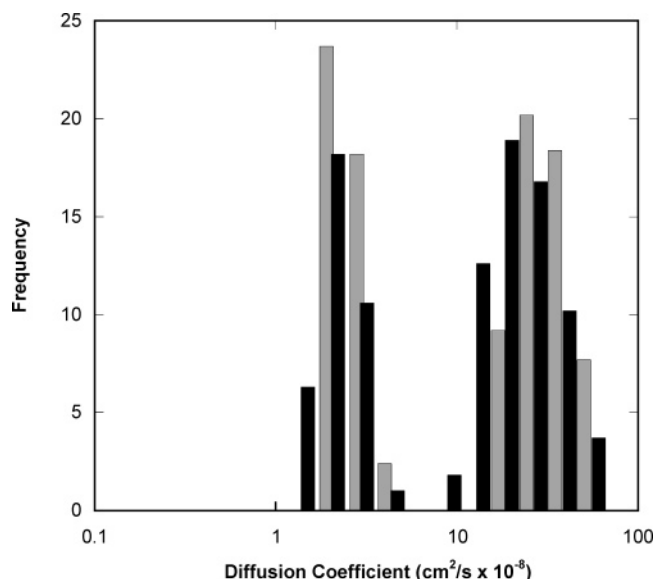
Substantial differences are observed between the scattering curves for 19 mM SDS (Figure 5), and the mixed system PNAA/SDS (1:19 mM, Figure 6). Since SDS is known to form spherical micelles, data was fitted using a core−shell spherical model including polydispersity. Using literature values for the scattering
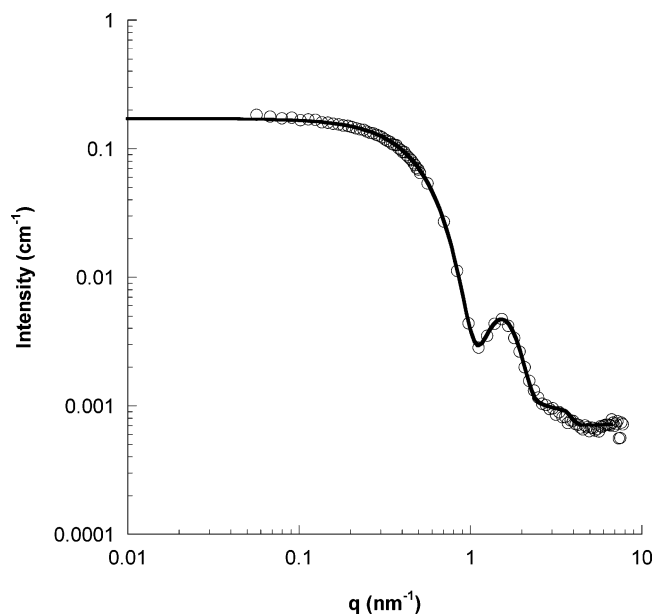
Figure 7. Synchrotron SAXS intensities for scattering from 1 mM PNAA in 50 mM Tris-HCl buffer (pH 8.0). The solid line is a fit to a monodisperse core−shell prolate ellipsoid model (eq 10) with the fit parameters in Table 2. Only 1 of every 10 data points is plotted for ease of viewing.

Figure 8. Diffusion coefficient distributions from dynamic light scattering from 1 mM PNAA in 50 mM Tris-HCl buffer (pH 8.0). The slow mode is presumed to result from vesicles and other large structures brought about by filtration (see text). Solutions were centrifuged at ∼10 000g, and DLS measurements were taken immediately after centrifugation (gray) and after one week (black).

cross section of the core and shell and allowing other parameters of eq 8 (Table 2) to vary, an average micelle radius of $R_s = 2.09$ nm was obtained, consistent with literature values.[9] The scattering curve of PNAA/SDS mixed micelles is qualitatively similar to that of pure SDS. Similar model fitting (Table 2) shows that the addition of PNAA to SDS yields spherical mixed micelles with a slightly larger size ($R_s = 2.67$ nm). The existence of a single population of mixed PNAA/SDS micelles agrees with the CE results (Figure 4a), which show a marked increase in electrophoretic mobility on addition of 19 mM SDS to 1 mM PNAA and the presence of a single population for the mixed system. It should be noted that the SDS has negligible absorbance at 254 nm and is undetectable by the CE detector.

The dye solubilization data presented above confirms that PNAA form micelles at concentrations above ca. 100 μM in our pH 8.0 buffer. Due to instrumental limitations, we were not able to obtain sufficient signal in the low-q regime to confidently assign a morphology and size to the PNAA micelles. Synchrotron X-ray studies provided a much greater q range to enable fitting (Figure 7). Here, it can be seen that the low-q data levels out at $q = 0.1$ nm^{-1}, suggesting short ellipsoidal micelles. The scattering curve was fit very well using a core−shell prolate ellipsoid model with the dimensions given in Table 2. A complication in the fitting procedure is that the scattering cross section (ρ) and the particle density (N_p) are perfectly correlated (eq 10−13) and cannot be distinguished without additional data. In the case of pure SDS and SDS + PNAA (Figures 5 and 6), we could use literature values to check ρ for physical reasonableness. For the case of pure PNAA micelles, we cannot assume that the core is solid hydrocarbon, nor can

we assume that ρ_{shell} will be identical to that for SDS micelles. The values of Table 2 are simply a combination of physically reasonable values of ρ and N_p that give a good fit. Even so, the obtained core density is about half what would be expected for a solid hydrocarbon, suggesting a loosely packed arrangement of peptide and hydrocarbon. We emphasize that the micelle dimensions (R_{maj} and R_{min}, etc.) are independent variables unlike ρ and N_p.

Given the total concentration of surfactant added ([surf], on a monomer basis), the aggregation number (N_{agg}) of the micelles can be calculated as follows:

$$N_{agg} = \frac{[surf] - CMC}{N_p} \qquad (18)$$

Table 3 summarizes the values for each of the micellar systems. Values for N_{agg} are in good agreement with that expected for pure SDS. On addition of 1 mM PNAA, N_{agg} doubles as expected for the larger volume of micelles obtained for the mixed SDS/PNAA system. N_{agg} for the pure PNAA system is not obtainable for the reasons listed above, but the calculated value is tabulated for completeness. It should also be noted that the broad monomer-to-micelle transition of Figure 2 suggests that the micelles are quite polydisperse; however, fits to the scattering data of Figure 7 were not improved by considering polydispersity of the axial ratio or polydispersity of the overall micelle size.

Size Scales of PNAA Micelles Determined by Dynamic Light Scattering (DLS). To support the morphological and size characterization provided by SAXS, dynamic light scattering

TABLE 2: Best Fit Parameters from the Polydisperse, Core−Shell Spherical Model (SDS, PNAA + SDS, Equation 8) and the Monodisperse, Core−Shell Prolate Ellipsoid Model (PNAA, Equation 10)

	R_c (nm)	R_s (nm)	σ	ρ_{core} (nm^{-2})	ρ_{shell} (nm^{-2})	ρ_{solv} (nm^{-2})	N_p (nm^{-3})	
SDS	1.71	2.09	0.09	7.81×10^{-4}	12.8×10^{-4}	9.46×10^{-4}	1.62×10^{-4}	
PNAA/SDS	1.97	2.67	0.175	7.81×10^{-4}	11.7×10^{-4}	9.46×10^{-4}	9.54×10^{-5}	

	$R_{c,maj}$ (nm)	$R_{c,min}$ (nm)	$R_{s,maj}$ (nm)	$R_{s,min}$ (nm)	a/b	ρ_{core} (nm^{-2})	ρ_{shell} (nm^{-2})	ρ_{solv} (nm^{-2})	N_p (nm^{-3})	bk$g$
PNAA	1.05	0.90	5.15	3.20	1.61	4.46×10^{-4}	10.5×10^{-4}	9.46×10^{-4}	4.30×10^{-5}	0.0007

Self-Assembled Peptide Nucleic Acid Amphiphiles

J. Phys. Chem. B, Vol. 110, No. 18, 2006 **9033**

TABLE 3: Size and Aggregation Numbers (N_{agg}) for the Micelles Characterized in This Study

	N_p (mM)	[surf] (mM)	CMC (mM)	N_{agg}
SDS	0.267	19	3.0	59.3
PNAA+SDS	0.158	20	3.0[a]	107
PNAA	0.0714[b]	1	0.111	12.5[b]

[a] For the mixed system of 1 mM PNAA and 19 mM SDS, the CMC was taken to be that of pure SDS and the total concentration of surfactant in micelles was taken to be 17 mM ([PNAA] + [SDS]-CMC, SDS). [b] Since the contrast factors and *scale* are perfectly correlated, only one can be varied during the fit of eqs 10–13. Since the core electron density, shell electron density, and scale are all unknowns in the system, we simply picked one of many physically reasonable combinations of these values. Note that the dimensions of the micelle are not impacted by this ambiguity.

TABLE 4: Comparison of DLS-Derived Diffusion Coefficients with Theoretical Values from SAXS-Derived Micelle Dimensions (Equations 16 and 17)

	D_{app} (10^{-8} cm^2/s)	D_{theo} (10^{-8} cm^2/s)
SDS	116	117
PNAA/SDS	110	96.8
PNAA	51.6	65.0

(DLS) studies were also carried out (Figure 8). These measurements give the diffusion coefficient, which can then be compared to those expected from the SAXS size and shape data. For the PNAA micelles ([PNAA] = 1 mM, 50 mM Tris-HCl, pH 8.0), CONTIN analysis of the autocorrelation function gave a bimodal distribution, with one peak centered at 4×10^{-8} cm^2/s and a second centered at 50×10^{-8} cm^2/s. The slow mode of the spectrum can be attributed to the formation of vesicles and other large-scale structures brought about by the filtration required to remove dust particles. This observation has been made previously for the characterization of nonionic surfactant micelles by DLS,[24,26] and the slow mode was not observed when using ultracentrifugation rather than filtration. We note that such filtration was not required for the SAXS analysis presented here.

Using the fast-mode result of $D_{app} = 51.6 \times 10^{-8}$ cm^2/s and the SAXS-derived values for the axial ratio and semimajor axis length, eq 17 predicts an infinite-dilution diffusion coefficient of $D_{app} = 65.0 \times 10^{-8}$ cm^2/s, well within the distribution of Figure 8. Analysis of D_{app} for SDS and PNAA/SDS mixed micelles also gives good agreement between the measured values and those calculated for spheres using the SAXS-derived shell radii (Table 4).

Conclusions

By a combination of low- and high-energy SAXS along with DLS, we have shown that the peptide nucleic acid amphiphile C_{12}-tagacg-$(E)_2$ forms ellipsoidal micelles above its critical micelle concentration of 110.9 μM. On addition of 19 mM SDS, swollen spherical mixed micelles of PNAA and SDS are formed.

On addition of DNA, PNAA in its pure micelle form, or in mixed micelles with SDS, hybridizes to DNA. The resulting PNAA/DNA duplex transfers from the micelle pseudophase to the solvent phase as judged by capillary electrophoresis and dye solubilization studies. Future work will focus on methods to retain the PNAA/DNA duplexes in micelles for higher-resolution separations.

References and Notes

(1) Gore, T.; Dori, Y.; Talmon, Y.; Tirrell, M.; Bianco-Peled, H. *Langmuir* **2001**, *17*, 5352.
(2) Hartgerink, J. D.; Beniash, E.; Stupp, S. I. *Science* **2001**, *294*, 1684.
(3) Shimizu, T.; Hato, M. *Biochim. Biophys. Acta* **1993**, *1147*, 50.
(4) Long, M. A.; Kaler, E. W.; Lee, S. P.; Wignall, G. D. *J. Phys. Chem.* **1994**, *98*, 4402.
(5) Galantini, L.; Giglio, E.; Leonelli, A.; Pavel, N. V. *J. Phys. Chem. B* **2004**, *108*, 3078.
(6) Chu, B.; Liu, T. *J. Nanopart. Res.* **2000**, *2*, 29.
(7) Castelletto, V.; Hamley, I. W. *Curr. Opin. Colloid Interface Sci.* **2002**, *7*, 167.
(8) He, L.; Garamus, V. M.; Funari, S. S.; Malfois, M.; Willumeit, R.; Niemeyer, B. *J. Phys. Chem. B* **2002**, *106*, 7596.
(9) Zemb, T.; Charpin, P. *J. Phys.* **1985**, *46*, 249.
(10) Imae, T.; Kayashi, B.; Matsumoto, T.; Tada, T.; Furusaka, M. *J. Colloid Interface Sci.* **2000**, *225*, 285.
(11) Vernille, J. P.; Kovell, L. C.; Schneider, J. W. *Bioconjugate Chem.* **2004**, *15*, 1314.
(12) Vernille, J. P.; Schneider, J. W. *Biotechnol. Prog.* **2004**, *20*, 1776.
(13) Marques, B. F.; Schneider, J. W. *Langmuir* **2005**, *21*, 2488.
(14) Nielsen, P. E. *Acc. Chem. Res.* **1999**, *32*, 624.
(15) Quirino, J. P.; Terabe, S. *J. Chromatogr., A* **1997**, *781*, 119.
(16) Quirino, J. P.; Terabe, S. *Science* **1998**, *282*, 465.
(17) Nielsen, P. E.; Egholm, M. *Peptide Nucleic Acids Protocols and Applications*; Horizon Scientific Press: Wymondham, U.K., 1999.
(18) Evans, D. F.; Wennerstrom, H. *The Colloidal Domain*; Wiley-VCH: New York, 1999.
(19) Wächter, A.; Biegler, L. T. *Math. Programming* **2005**, in press.
(20) Stabinger, H.; Kratky, O. *Makromol. Chem.* **1978**, *179*, 1655.
(21) Glatter, O.; Kratky, O. *Small Angle X-ray Scattering*; Academic Press INC: New York, 1982.
(22) Pedersen, J. S. *Adv. Colloid Interface Sci.* **1997**, *70*, 171.
(23) Caetano, W.; Barbosa, L. R. S.; Itri, R.; Tabak, M. *J. Colloid Interface Sci.* **2003**, *260*, 414.
(24) Thomas, H. G.; Lomakin, A.; Blankschtein, D.; Benedek, G. B. *Langmuir* **1997**, *13*, 209.
(25) Mikkers, F. E. P.; Everaerts, F. M.; Verheggen, P. E. M. *J. Chromatogr.* **1979**, *169*, 1.
(26) Brown, W.; Pu, Z.; Rymdén, R. *J. Phys. Chem.* **1988**, *92*, 6086.